

Anisotropic Mesh Adaptation for Finite Element Solution of Anisotropic Porous Medium Equation

Xianping Li*

Anisotropic Porous Medium Equation (APME) is developed as an extension of the Porous Medium Equation (PME) for anisotropic porous media. A special analytical solution is derived for APME for time-independent diffusion. Anisotropic mesh adaptation for linear finite element solution of APME is discussed and numerical results for two dimensional examples are presented. The solution errors using anisotropic adaptive meshes show second order convergence.

AMS 2010 Mathematics Subject Classification. 65M60, 65M50

Key words. porous medium equation, anisotropic mesh adaptation, adaptive mesh, anisotropic diffusion, finite element, moving mesh

1 Introduction

In this paper, we extend the porous medium equation (PME) to the Anisotropic Porous Medium Equation (APME) that takes into consideration the anisotropic physical properties of the porous media such as permeability. Then we study the linear finite element solution of APME. We consider the following problem

$$\begin{cases} u_t = \nabla \cdot (u^m \mathbb{D} \nabla u), & \text{in } \Omega_T = \Omega \times (t_0, T] \\ u(\mathbf{x}, t) = 0, & \text{on } \partial\Omega \times (t_0, T], \\ u(\mathbf{x}, 0) = u_0(\mathbf{x}), & \text{in } \Omega \times \{t = t_0\} \end{cases} \quad (1)$$

where $u = u(\mathbf{x}, t)$ is a nonnegative scalar function, $m \geq 1$ is the physical parameter, $\Omega \subset \mathbb{R}^d$ is a connected polygonal or polyhedral domain of d -dimensional space, $t_0 \geq 0$ is the starting time, $T > 0$ is the end time, $u_0(\mathbf{x}) \geq 0$ is a given function. We assume that $\mathbb{D} = \mathbb{D}(\mathbf{x})$ is a general symmetric and strictly positive definite matrix-valued function on Ω_T that takes both isotropic and anisotropic diffusion as special cases. For simplicity, we consider only time-independent diffusion matrix \mathbb{D} in this work. The principles can also be applied to the time-dependent situation with minor modifications.

Porous medium equation (PME) arises in many fields of science and engineering such as fluid flow in porous media, heat transfer or diffusion, image processing, and population dynamics [36]. The general form is given as

$$u_t = \nabla \cdot (\nabla u^{m+1}), \quad (2)$$

*Department of Mathematics and Statistics, the University of Missouri-Kansas City, Kansas City, MO 64110, U.S.A.
(lixianp@umkc.edu)

or in the modified form

$$u_t = \nabla \cdot (u^m \nabla u). \quad (3)$$

For gas flow in porous media, m is the heat capacity ratio, u represents the density, u^m is the pressure, and $-\nabla u^m$ is the velocity.

Mathematically, the parameter m in (3) can take any real value. Specifically, when $m = 0$, the PME (2) or (3) reduces to the heat equation. When $m > 0$, the PME becomes a nonlinear evolution equation of parabolic type that has attracted interests of both theoretical and computational mathematicians. Particularly, when $m = 1$, the PME is called the Boussinesq's equation that models groundwater flow in a porous stratum.

The nonlinear term u^m in (3) induces the so-called nonlinear diffusion that brings up many challenges in the analysis of the PME. However, this nonlinear diffusion is not the physical property of the porous media such as permeability. In this paper, we generalize PME to Anisotropic Porous Medium Equation (APME) that takes into account the anisotropy of the physical property of the porous media. In the mean time, APME can also be viewed as a nonlinear anisotropic diffusion problem.

General PME (2) or (3) has been studied extensively both in theory [28, 1, 19, 12, 13, 2, 34, 36] and numerical approximations [31, 6, 5, 37, 10, 38, 30, 11, 33, 7, 8, 22, 26]. In particular, the nonlinear diffusion term and the sharp gradient near the free boundary make it difficult to achieve high order convergence of the numerical solutions. For example, finite difference moving mesh method has been developed in [33, 22] for PME in one-dimensional space and second order convergence has been observed; however, no result is provided for PME in 2D. Error estimates have been developed in [30] for finite volume discretization of PME in 2D, which shows only first order convergence. For finite element discretization using quasi-uniform meshes [31, 27, 32, 9, 37], the convergence is at most first order for $m = 1$ and decreases for larger m . For one dimensional PME, high order convergence rate was achieved on a uniform mesh by using a high order local discontinuous Galerkin finite element method [38].

On the other hand, adaptive meshes and moving meshes are great choices to improve computational efficiency and accuracy by concentrating more mesh elements in the regions where solution changes significantly. In particular, Ngo and Huang [26] have studied moving mesh finite element solution of PME and demonstrated the advantages of moving mesh over quasi-uniform meshes. Their results show second-order convergence of solution errors using moving meshes.

However, no result is currently available for APME. Interesting features of PME also appear in APME such as finite propagation, free boundaries and waiting time phenomenon. Moreover, with the anisotropy of the porous media, satisfaction of maximum principle becomes more challenging and special mesh adaptation is needed, see [21, 23, 24] and the references therein. This paper serves as a starting effort about APME and its numerical solutions. Anisotropic mesh adaptation technique is applied in the numerical computations to improve efficiency and accuracy. Different than moving mesh method that keeps the connectivity of the elements, our anisotropic mesh adaptation technique can change the connectivity as well as the number of elements as desired. Therefore, a coarse uniform mesh can be used as the initial mesh in our adaptation, while a fine initial mesh is usually needed for moving mesh method in order to capture the sharp change of solution on the initial free boundary.

The outline of this paper is as follows. In Section 2, the anisotropic porous medium equation (APME) is developed and the exact solution for a special case is discussed. Section 3 gives a brief summary of linear finite element solution of the APME, and Section 4 introduces the anisotropic mesh adaptation methods. Numerical examples are presented in Section 5 to show the different behavior between APME and PME and also demonstrate the advantages of adaptive anisotropic meshes over other meshes. Finally, some conclusions are drawn in Section 6.

2 Anisotropic Porous Medium Equation (APME)

Firstly, we derive the model for fluid flow through anisotropic porous media as follows. Let u be the density of the fluid. The flow is governed by the following three equations.

(I) Conservation of mass (continuity equation)

$$\varepsilon u_t = -\nabla \cdot (u \mathbf{v}), \quad (4)$$

where $\varepsilon \in (0, 1)$ is the porosity of the media and \mathbf{v} is the velocity.

(II) Darcy's law in anisotropic porous media

$$\mathbf{v} = -\frac{1}{\mu} \mathbb{D} \nabla p, \quad (5)$$

where μ is the viscosity of the fluid, \mathbb{D} is the permeability matrix of the porous media, and p is the pressure. In most cases, the porous media is anisotropic, thus \mathbb{D} has different eigenvalues. If \mathbb{D} varies with location, then it also represents heterogeneous media.

(III) The equation of state

$$p = p_0 u^m, \quad (6)$$

where p_0 is the reference pressure and $m \geq 1$ is the ratio of specific heats.

Combine (4), (5), (6) together, we have

$$\begin{aligned} u_t &= \frac{p_0}{\varepsilon \mu} \nabla \cdot (u \mathbb{D} \nabla u^m) \\ &= \frac{p_0}{\varepsilon \mu} \nabla \cdot (\mathbb{D} u \cdot m \cdot u^{m-1} \nabla u) \\ &= \frac{m p_0}{\varepsilon \mu} \nabla \cdot (\mathbb{D} u^m \nabla u) \end{aligned} \quad (7)$$

$$= \frac{m p_0}{(m+1) \varepsilon \mu} \nabla \cdot (\mathbb{D} \nabla u^{m+1}). \quad (8)$$

Scale time t with the constant $\frac{m p_0}{(m+1) \varepsilon \mu}$ in (8) or $\frac{m p_0}{\varepsilon \mu}$ in (7), we obtain the anisotropic porous medium equation (APME) as follows

$$u_t = \nabla \cdot (\mathbb{D} \nabla u^{m+1}) \quad (9)$$

or

$$u_t = \nabla \cdot (u^m \mathbb{D} \nabla u). \quad (10)$$

Combining $u^m \mathbb{D}$ in (10) together as the diffusion term, APME can be viewed as an anisotropic diffusion equation with induced nonlinearity from the solution. Thus, available results for anisotropic diffusion problems [4, 35, 21, 23, 24] are useful for the study of APME.

Note that, Vázquez has mentioned the extension of PME in non-homogeneous media (NHPME) in [36] as

$$\varepsilon(\mathbf{x}, t) u_t = \nabla \cdot (c(\mathbf{x}, t) \nabla u^{m+1}), \quad (11)$$

where $\varepsilon(\mathbf{x}, t)$ and $c(\mathbf{x}, t)$ are nonnegative functions. However, the anisotropy of the porous media has not been considered in NHPME. In this sense, both PME (2) and NHPME (11) are special cases of APME (10), where both the anisotropy and heterogeneity are taken into account in the diffusion matrix \mathbb{D} .

Next, we derive a special solution for (1). We start with the Barenblatt-Pattle solution for PME (2) developed by Barenblatt [3] and Pattle [29] independently. Suppose the initial solution $u_0(\mathbf{x})$ (at time t_0) is compact-supported in a region given by $r_0 > 0$ as

$$u_0(\mathbf{x}) = \max \left\{ \left(1 - \frac{\mathbf{x}^T \mathbf{x}}{r_0^2} \right)^{\frac{1}{m}}, \quad 0 \right\}. \quad (12)$$

The solution at time $t \geq t_0$ for PME is given by

$$u(\mathbf{x}, t) = \max \left\{ \frac{1}{\kappa^d} \left(1 - \frac{\mathbf{x}^T \mathbf{x}}{r_0^2 \kappa^2} \right)^{\frac{1}{m}}, \quad 0 \right\}, \quad (13)$$

where

$$\kappa = \left(\frac{t}{t_0} \right)^\beta, \quad \beta = \frac{1}{dm + 2}, \quad \text{and} \quad t_0 = \frac{1}{2} \beta m r_0^2. \quad (14)$$

For APME, we consider the mesh \mathcal{T}_h in the physical domain Ω as a uniform mesh \mathcal{T}_c in the computational domain Ω_c specified by the metric \mathbb{M} . By choosing $\mathbb{M} = \mathbb{D}^{-1}$, the diffusion can be considered as isotropic in the computational domain Ω_c with mesh \mathcal{T}_c [17, 23]. We apply the Barenblatt-Pattle solution for PME in Ω_c and then map the solution to Ω for APME. Denote the vertices in \mathcal{T}_c by $\tilde{\mathbf{x}}$, we have

$$\tilde{\mathbf{x}} = \mathbb{M}^{\frac{1}{2}} \mathbf{x} = \mathbb{D}^{-\frac{1}{2}} \mathbf{x}. \quad (15)$$

We also consider the initial solution in a region given by $r_0 > 0$ in Ω_c as

$$u_0(\mathbf{x}) = \max \left\{ \left(1 - \frac{\tilde{\mathbf{x}}^T \tilde{\mathbf{x}}}{r_0^2} \right)^{\frac{1}{m}}, \quad 0 \right\} = \max \left\{ \left(1 - \frac{\mathbf{x}^T \mathbb{D}^{-1} \mathbf{x}}{r_0^2} \right)^{\frac{1}{m}}, \quad 0 \right\}. \quad (16)$$

Then the solution at time $t \geq t_0$ for APME is given by

$$\begin{aligned} u(\mathbf{x}, t) &= \max \left\{ \frac{1}{\kappa^d} \left(1 - \frac{\tilde{\mathbf{x}}^T \tilde{\mathbf{x}}}{r_0^2 \kappa^2} \right)^{\frac{1}{m}}, \quad 0 \right\} \\ &= \max \left\{ \frac{1}{\kappa^d} \left(1 - \frac{\mathbf{x}^T \mathbb{D}^{-1} \mathbf{x}}{r_0^2 \kappa^2} \right)^{\frac{1}{m}}, \quad 0 \right\} \end{aligned} \quad (17)$$

where κ , β , and t_0 are the same as those defined in (14).

Remark 2.1. If the initial solution of APME is taken as (12) instead of (16), the boundary of the compact support is not a circle in the computational domain Ω_c . Therefore, the evolution of the solution cannot be described by the solution (17). The difference will be demonstrated in Examples 5.1 and 5.2.

3 Linear finite element formulation

In this section, we briefly describe the linear finite element formulation of IBVP (1). Assume that an affine family of simplicial triangulations $\{\mathcal{T}_h\}$ is given for the physical domain Ω , and define

$$U_0 = \{v \in H^1(\Omega) \mid v|_{\partial\Omega} = 0\}.$$

Denote the linear finite element space associated with mesh \mathcal{T}_h by U_0^h . Then a linear finite element solution $u^h(t) \in U_0^h$ for $t \in (0, T]$ to IBVP (1) is defined by

$$\int_{\Omega} \frac{\partial u^h}{\partial t} v^h d\mathbf{x} + \int_{\Omega} (\nabla v^h)^T \left((u^h)^m \mathbb{D} \right) \nabla u^h d\mathbf{x} = 0, \quad \forall v^h \in U_0^h, \quad t \in (t_0, T]. \quad (18)$$

Denote the numbers of the elements, vertices, and interior vertices of \mathcal{T}_h by N , N_v , and N_{vi} , respectively. Assume that the first N_{vi} vertices are the interior vertices. Then U_0^h and u^h can be expressed as

$$\begin{aligned} U_0^h(t) &= \text{span}\{\phi_1, \dots, \phi_{N_{vi}}\}, \\ u^h &= \sum_{j=1}^{N_{vi}} u_j(t) \phi_j + \sum_{j=N_{vi}+1}^{N_v} u_j(t) \phi_j, \end{aligned} \quad (19)$$

where ϕ_j is the linear basis function associated with the j^{th} vertex, \mathbf{x}_j , at time t . The boundary and initial conditions in (1) are approximated as

$$u_j(t) = 0, \quad j = N_{vi} + 1, \dots, N_v, \quad (20)$$

and

$$u_j(t_0) = u_0(\mathbf{x}_j), \quad j = 1, \dots, N_v. \quad (21)$$

Substituting (19) into (18), taking $v^h = \phi_i$ ($i = 1, \dots, N_{vi}$), and combining the resulting equations with (20), we obtain the linear algebraic system

$$M \frac{d\mathbf{u}}{dt} + A(u^h) \mathbf{u} = \mathbf{0}, \quad (22)$$

where $\mathbf{u} = (u_1, \dots, u_{N_{vi}}, u_{N_{vi}+1}, \dots, u_{N_v})^T$ is the unknown vector and M and A are the mass and stiffness matrices, respectively. The entries of the matrices are given as follows. For $j = 1, \dots, N_v$,

$$m_{ij} = \begin{cases} \int_{\Omega} \phi_j \phi_i d\mathbf{x} = \sum_{K \in \mathcal{T}_h} \int_K \phi_j \phi_i d\mathbf{x}, & i = 1, \dots, N_{vi} \\ 0, & i = N_{vi} + 1, \dots, N_v \end{cases} \quad (23)$$

$$a_{ij} = \begin{cases} \int_{\Omega} (\nabla \phi_i)^T (u^h)^m \mathbb{D} \nabla \phi_j d\mathbf{x} = \sum_{K \in \mathcal{T}_h} \int_K (\nabla \phi_i)^T (u^h)^m \mathbb{D} \nabla \phi_j d\mathbf{x}, & i = 1, \dots, N_{vi} \\ \delta_{ij}, & i = N_{vi} + 1, \dots, N_v. \end{cases} \quad (24)$$

The system (22) is solved using the fifth-order Radau IIA method with a two-step error estimator [14]. The relative and absolute tolerances are chosen as 10^{-6} and 10^{-8} , respectively.

Next, we apply the anisotropic mesh adaptation method to generate the mesh \mathcal{T}_h^n for time $t = t^n$ ($n = 0, 1, \dots$).

4 Anisotropic mesh adaptation

In this section we briefly introduce the anisotropic mesh adaptation method used in the computations for this paper. More details about the method can be found in [16, 17, 23, 18]. We take the so-called \mathbb{M} -uniform mesh approach where an adaptive mesh is viewed as a uniform one in the metric specified

by a tensor $\mathbb{M} = \mathbb{M}(\mathbf{x})$ that is assumed to be symmetric and uniformly positive definite on Ω . It is shown in [17] that an \mathbb{M} -uniform mesh \mathcal{T}_h satisfies

$$|K| \det(\mathbb{M}_K)^{\frac{1}{2}} = \frac{\sigma_h}{N}, \quad \forall K \in \mathcal{T}_h \quad (25)$$

$$\frac{1}{d} \text{tr}((F'_K)^T \mathbb{M}_K F'_K) = \det((F'_K)^T \mathbb{M}_K F'_K)^{\frac{1}{d}}, \quad \forall K \in \mathcal{T}_h \quad (26)$$

where

$$\mathbb{M}_K = \frac{1}{|K|} \int_K \mathbb{M}(\mathbf{x}) d\mathbf{x}, \quad \sigma_h = \sum_{K \in \mathcal{T}_h} \det(\mathbb{M}_K)^{\frac{1}{2}} |K|. \quad (27)$$

Condition (25) is called as *the equidistribution condition* which determines the size of K from $\det(\mathbb{M}_K)^{\frac{1}{2}}$, while (26) is called *the alignment condition* which controls the shape and orientation of K .

In this paper, we consider three choices of metric tensors for adaptive meshes. The first choice is based on minimization of the H^1 semi-norm of linear interpolation error and is given in [16] by

$$\mathbb{M}_{adap}(K) = \left\| I + \frac{1}{\alpha_h} |H_K(u^h)| \right\|^{\frac{2}{5}} \det \left(I + \frac{1}{\alpha_h} |H_K(u^h)| \right)^{-\frac{1}{5}} \left[I + \frac{1}{\alpha_h} |H_K(u^h)| \right], \quad (28)$$

where u^h is the finite element solution, $H_K(u^h)$ is a recovered Hessian of u^h over K , $|H_K(u^h)|$ is the eigen-decomposition of $H_K(u^h)$ with the eigenvalues being replaced by their absolute values, and α_h is a positive regularization parameter.

The second and third choices are related to the diffusion matrix and are defined in [23] as

$$\mathbb{M}_{DMP}(K) = \mathbb{D}_K^{-1}, \quad \forall K \in \mathcal{T}_h \quad (29)$$

and

$$\mathbb{M}_{DMP+adap}(K) = \left(1 + \frac{1}{\alpha_h} B_K \right)^{\frac{2}{d+2}} \det(\mathbb{D}_K)^{\frac{1}{d}} \mathbb{D}_K^{-1}, \quad (30)$$

where

$$\begin{aligned} \mathbb{D}_K &= \frac{1}{|K|} \int_K \mathbb{D}(\mathbf{x}) d\mathbf{x}, \\ B_K &= \det(\mathbb{D}_K)^{-\frac{1}{d}} \|\mathbb{D}_K^{-1}\| \cdot \|\mathbb{D}_K |H_K(u^h)|\|^2, \\ \alpha_h &= \left(\frac{1}{|\Omega|} \sum_{K \in \mathcal{T}_h} |K| B_K^{\frac{d}{d+2}} \right)^{\frac{d+2}{d}}. \end{aligned}$$

The \mathbb{M} -uniform meshes associated with \mathbb{M}_{DMP} and $\mathbb{M}_{DMP+adap}$ satisfy the alignment condition (26), and the mesh elements are aligned along the principal diffusion direction that is the direction of the eigenvector corresponding to the largest eigenvalue of the diffusion matrix \mathbb{D} .

If only fixed mesh is used in the computations, a very fine initial mesh is needed in order to capture the sharp change of solution at the initial free boundary. Even for moving mesh methods, an initial fine mesh is usually needed since the connectivity of the mesh elements is fixed. For adaptive meshes, however, they only need to concentrate elements around the initial free boundary or moving boundary. Therefore, an anisotropic initial mesh will significantly increase the efficiency and accuracy of the computation. The anisotropic initial mesh can be generated by adapting a uniform Delaunay

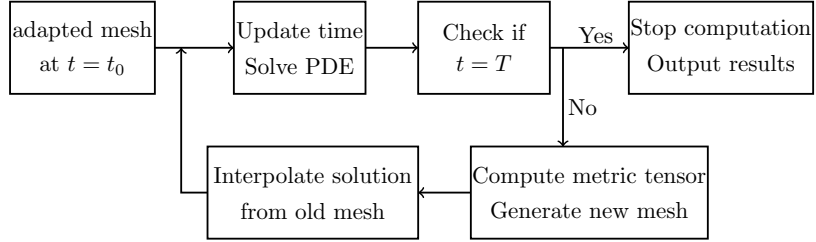


Figure 1: Procedures for anisotropic mesh adaptation based on \mathbb{M} -uniform mesh approach

mesh according to a metric tensor \mathbb{M} . The adaptation can iterate a few times to generate an initial mesh with good quality.

Starting with the adapted initial mesh, the procedures for anisotropic mesh adaptation based on \mathbb{M} -uniform mesh is shown in Fig. 1. Some numerical results are presented in the next section.

Remark 4.1. In the mesh adaptation procedures shown in Fig. 1, we use linear finite element interpolation to map the solution from old mesh to the new adaptive mesh for the current time t^n . Then the new mesh is used to solve PDE for the next time t^{n+1} . Higher order interpolations can also be used if needed.

Remark 4.2. The adaptation for the mesh at a given time t^n can be iterated a few times. However, the solution also needs to be interpolated correspondingly, which may reduce the accuracy of the solution. Therefore, the mesh is only adapted once for each time step in our computations.

Remark 4.3. Comparing to uniform meshes, the condition numbers of mass matrix M in (23) and stiffness matrix A in (24) for anisotropic meshes are affected by mesh non-uniformity. However, the condition numbers are still bounded. In anisotropic meshes, elements are usually concentrated in a small portion of the physical domain. With Jacobi preconditioning, the condition numbers of M and A for \mathbb{M} -uniform meshes are comparable with Delaunay meshes [20] and the impact on iterative convergence is not significant.

5 Numerical results

In this section we present numerical results obtained in two dimensions for three examples to demonstrate the different behavior between PME and APME as well as the significance of mesh adaptation in the computations. For comparison purpose, we consider four types of meshes. One is a fixed mesh that does not change through out the computations. The other three meshes are \mathbb{M}_{adap} mesh, \mathbb{M}_{DMP} mesh, and $\mathbb{M}_{DMP+adap}$ mesh that have been introduced in Section 4.

The fixed mesh is generated by splitting the rectangle domain into sub-rectangles, then each sub-rectangles are divided into four triangles by the diagonal lines. The adaptive meshes are generated using the Bidimensional Anisotropic Mesh Generator (BAMG) developed by Hecht [15] based on the Delaunay triangulation and local node movement.

Example 5.1. The first example is in the form of IBVP (1) for $m = 1$ on domain $\Omega = [-3, 3]^2$ with diffusion $\mathbb{D} = \begin{pmatrix} 5.5 & 4.5 \\ 4.5 & 5.5 \end{pmatrix}$ and u_0 given in (16) with $r_0 = 0.5$. The initial time is $t_0 = 0.03125$ by (14). The diffusion matrix has eigenvalues 10 and 1, and the principal eigenvectors are in the northeast

direction. The boundary of the support region for the initial solution is an ellipse in the physical domain Ω .

Fig. 2 shows the four different initial meshes obtained using different metric tensors for the computations. For \mathbb{M}_{adap} mesh, if not specified otherwise, the regularization parameter in (28) is chosen as $\alpha_h = 0.01$. As can be seen, the elements in both \mathbb{M}_{DMP} mesh and $\mathbb{M}_{DMP+adap}$ mesh are aligned along the north-east direction.

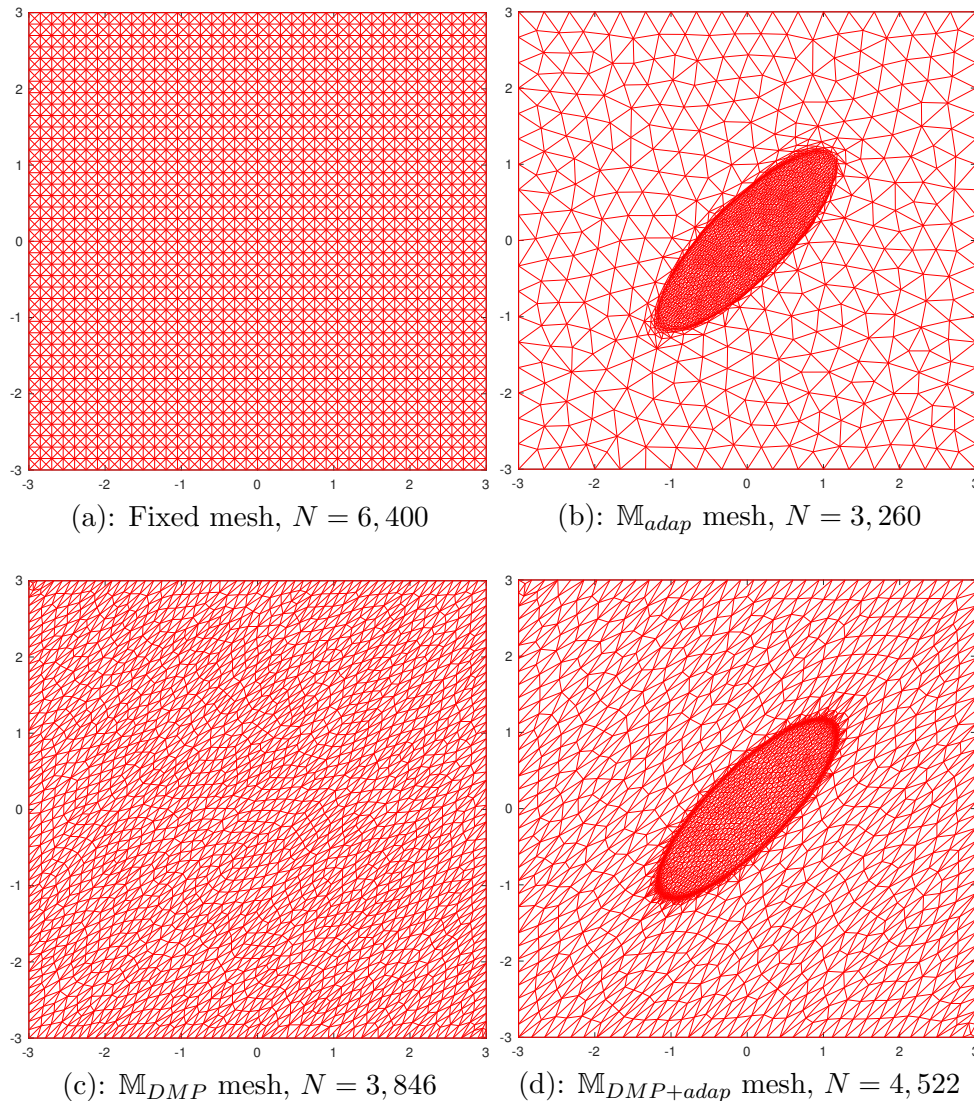


Figure 2: Example 5.1. Initial meshes generated using different metric tensors.

The initial solution at $t = t_0$ and the final solution at $t = 0.2$ are shown in Fig. 3. The \mathbb{M}_{adap} and $\mathbb{M}_{DMP+adap}$ meshes at different times are shown in Fig. 4. Comparing with the initial meshes in Fig. 2(b) and (d), it is clear that the free boundary moves outward in the shape of an ellipse in the physical domain and the meshes are adapted accordingly.

Remark 5.1. From the definition of metric tensors (28) and (30), the smaller α_h (hence larger $1/\alpha_h$), the more elements will be concentrated around the region with sharp change of solution. Fig. 5 shows \mathbb{M}_{adap} meshes obtained using $\alpha_h = 1$ at $t = t_0$ and $t = 0.06$. Comparing with Fig. 2(b) and

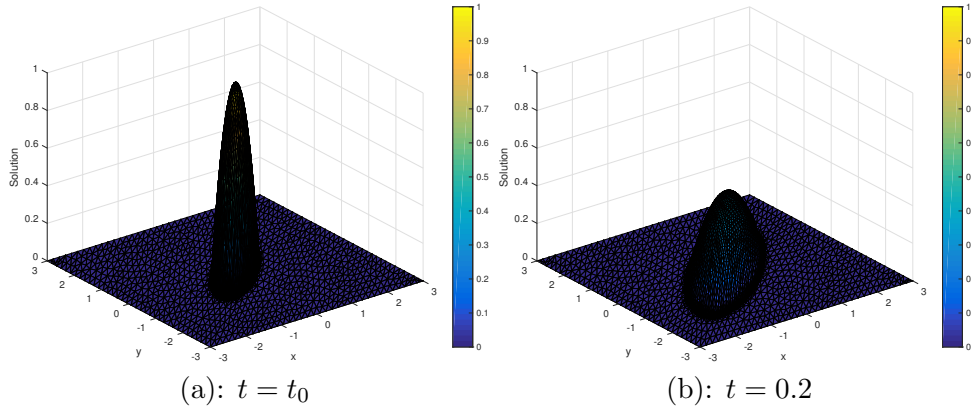


Figure 3: Example 5.1. Numerical solutions at different times.

Fig. 4(a), it is clear that $\alpha_h = 0.01$ provides better adaptation than $\alpha_h = 1$ for \mathbb{M}_{adap} .

For convergence of solution errors, we choose the final time as $T = (t_0 + 0.1)/2 = 0.065625$. The L^2 norm of the solution errors obtained from different meshes are plotted in Fig. 6, where $\mathbb{M}_{adap,1}$ and $\mathbb{M}_{adap,0.01}$ represent the results from \mathbb{M}_{adap} meshes obtained using $\alpha_h = 1$ and $\alpha_h = 0.01$, respectively. For comparison purpose, the first order and second order reference rates are also plotted in Fig. 6 and computed as $0.1/\sqrt{N}$ and $1/N$, respectively.

As can be seen from Fig. 6, the solution errors obtained from fixed mesh and \mathbb{M}_{DMP} mesh have first order convergence, with \mathbb{M}_{DMP} mesh providing smaller errors than fixed mesh. On the other hand, the errors obtained from \mathbb{M}_{adap} (both $\mathbb{M}_{adap,1}$ and $\mathbb{M}_{adap,0.01}$) and $\mathbb{M}_{DMP+adap}$ meshes have second order convergence, with $\mathbb{M}_{adap,0.01}$ mesh providing smallest errors.

It is interesting to observe that with slight adaptation using \mathbb{M}_{adap} meshes with $\alpha_h = 1$ (that is, $\mathbb{M}_{adap,1}$), the convergence rate of the solution errors has already been improved to second order. With better adaptation using $\alpha_h = 0.01$, the solution errors are not only of second order convergence but also much smaller than others.

The result demonstrates that adaptive meshes help the numerical solutions to achieve higher order convergence. In the mean time, $\mathbb{M}_{DMP+adap}$ mesh also performs well as a combination of \mathbb{M}_{DMP} and \mathbb{M}_{adap} , and the errors are between those from $\mathbb{M}_{adap,1}$ and $\mathbb{M}_{adap,0.01}$ meshes.

Remark 5.2. Similar to the effect of α_h for \mathbb{M}_{adap} meshes, the regularization parameter α_h in (30) for $\mathbb{M}_{DMP+adap}$ meshes can also be adjusted to improve the numerical solutions.

Example 5.2. The second example is the same as Example 5.1 except that the initial solution u_0 is defined as in (12) where the initial free boundary is a circle with radius r_0 in the physical domain Ω . The purpose of this example is to show the different behavior between our APME and general PME. For PME, as we know from the exact solution (13), the free boundary will move outward in a shape of a circle. However, it is not the case for APME.

Fig. 7 shows the initial and final meshes adapted from metric tensors \mathbb{M}_{adap} with $\alpha_h = 0.01$ and $\mathbb{M}_{DMP+adap}$. The solutions at different times are shown in Fig. 8. As can be seen from the meshes in Fig. 7, the free boundary varies from a circle gradually to an ellipse. At a given time, the elliptical boundary is different than the ones in Example 5.1 as shown in Fig. 4 (b) and (d). In particular, the eccentricity of the elliptical boundary is smaller than that in Example 5.1. The solution at $t = 0.2$ shown in Fig. 8(b) is also different than the one in Example 5.1 as shown in Fig. 3(b).

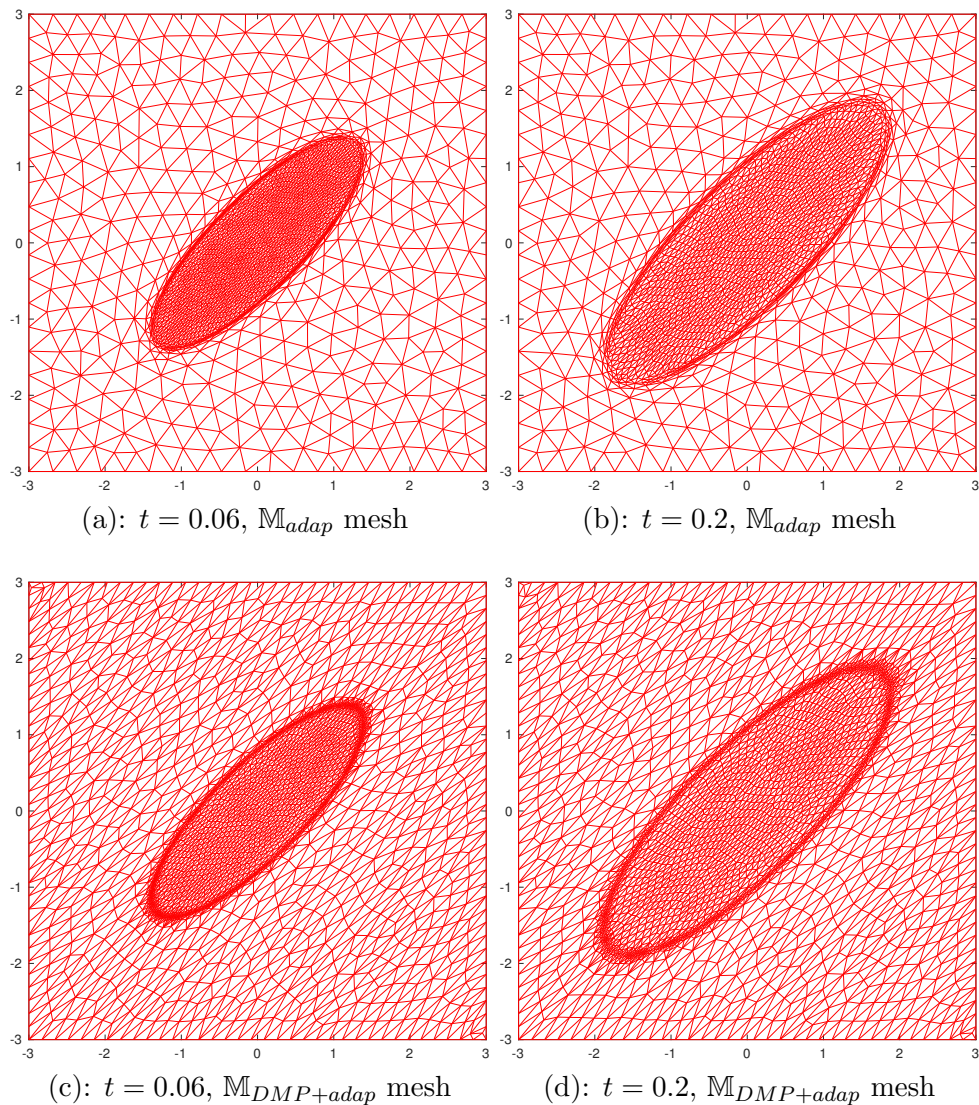


Figure 4: Example 5.1. \mathbb{M}_{adap} and $\mathbb{M}_{DMP+adap}$ meshes at different times.

For investigation purpose, the results for $m = 2$ using the same initial solutions are presented in Fig. 9. The observations are similar to the results for $m = 1$ except that the free boundary has not moved as much as that for $m = 1$ during the same time period.

Example 5.3. In the third example, we choose $m = 6$ and consider an initial solution with two-isolated support in domain $\Omega = [-3, 3]^2$. We also consider heterogeneous anisotropic diffusion. The initial solution is defined at $t_0 = 0$ as

$$u_0 = \begin{cases} 1, & \mathbf{x} \in \Omega_1 = (1, 2) \times (0, 1), \\ 1, & \mathbf{x} \in \Omega_2 = (-2, -1) \times (0.5, 1.5) \\ 0, & \mathbf{x} \in \Omega \setminus (\Omega_1 \cup \Omega_2). \end{cases} \quad (31)$$

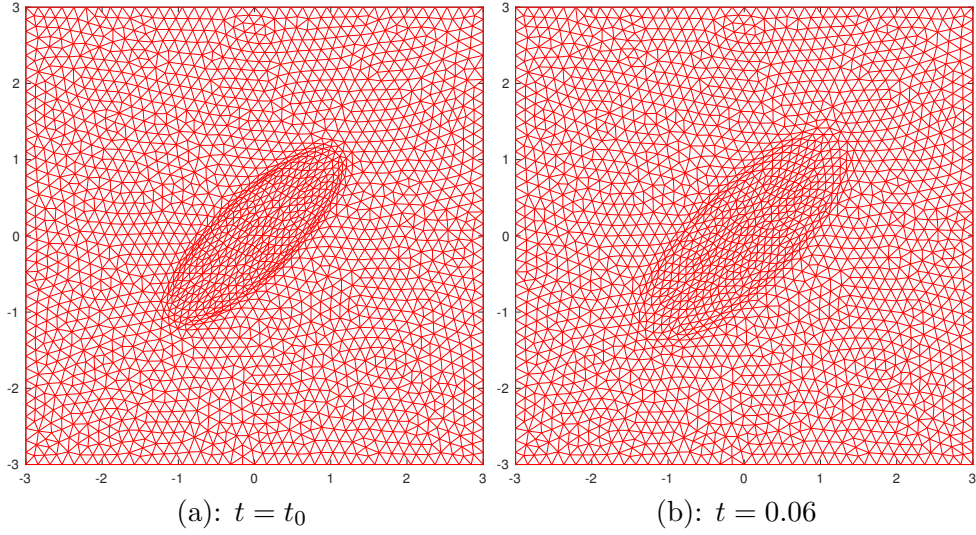


Figure 5: Example 5.2. \mathbb{M}_{adap} meshes obtained with $\alpha_h = 1$ at different times.

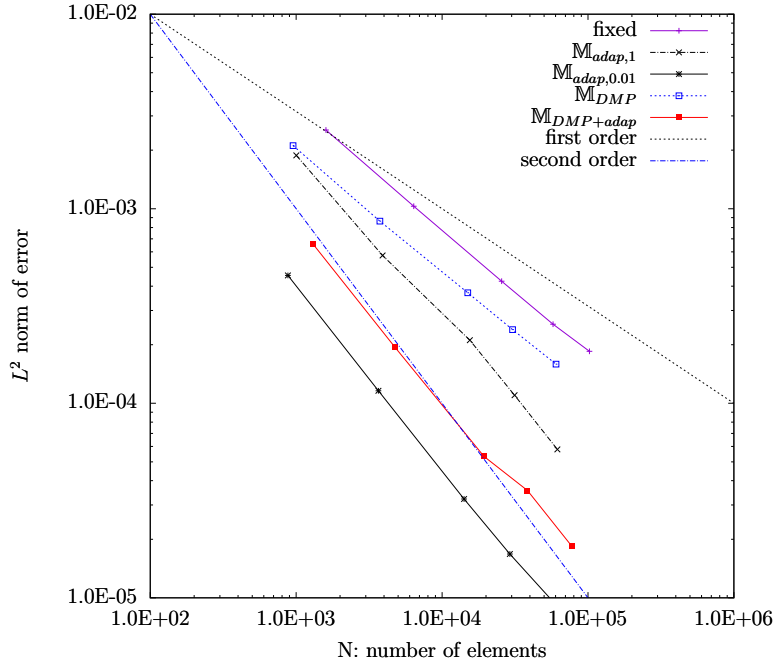


Figure 6: Example 5.1. L^2 norm of solution errors obtained from different meshes.

The end of time evolution is chosen as $T = 120$. The diffusion matrix $\mathbb{D} = \mathbb{D}(\mathbf{x})$ is taken as

$$\mathbb{D}(\mathbf{x}) = \begin{pmatrix} \cos \theta & -\sin \theta \\ \sin \theta & \cos \theta \end{pmatrix} \begin{pmatrix} 50 & 0 \\ 0 & 1 \end{pmatrix} \begin{pmatrix} \cos \theta & \sin \theta \\ -\sin \theta & \cos \theta \end{pmatrix}, \quad (32)$$

where $\theta = \theta(x, y) = \pi \sin(0.2x) \cos(0.1y)$ is the angle between the direction of the principle eigenvector

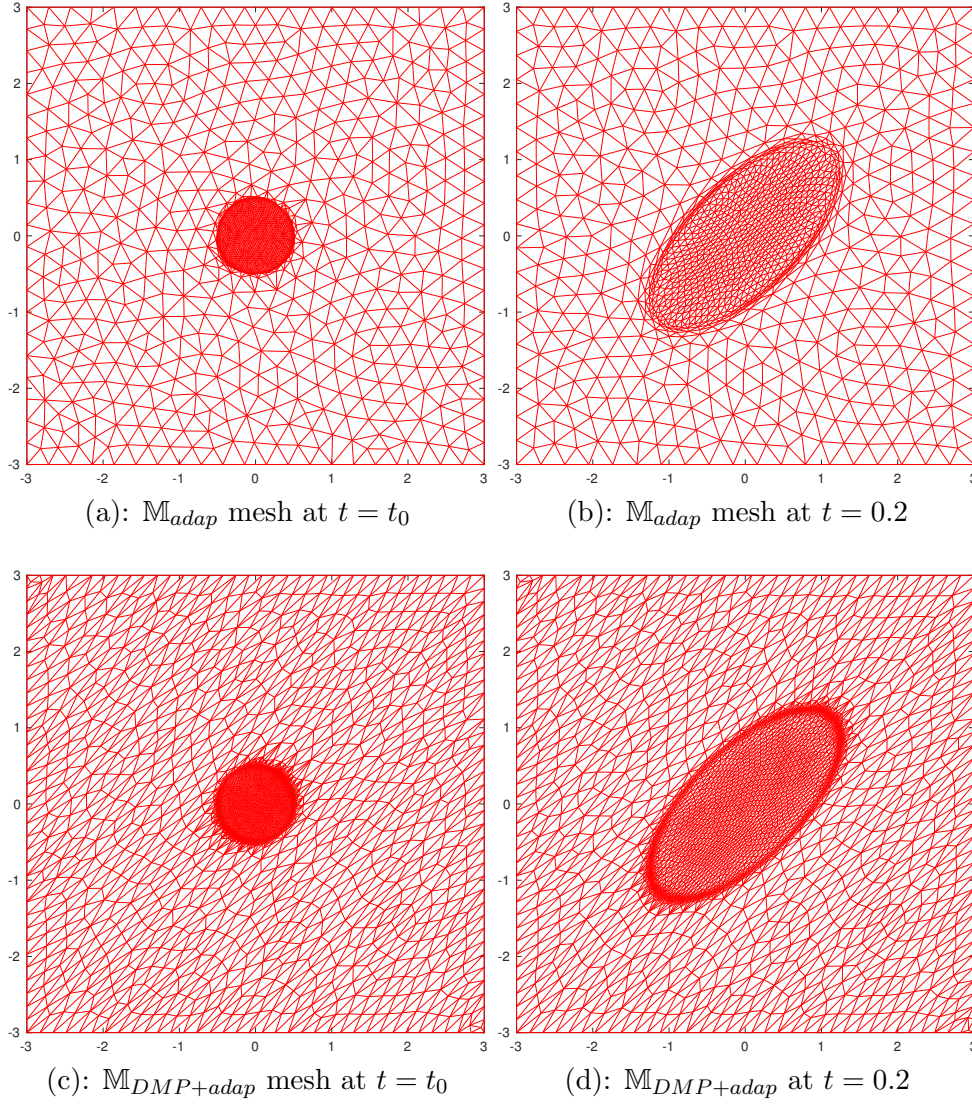


Figure 7: Example 5.2. \mathbb{M}_{adap} and $\mathbb{M}_{DMP+adap}$ meshes at different times, $m = 1$.

of \mathbb{D} and the positive x -axis. With this choice of θ , the primary diffusion direction changes at different locations.

The initial and final solutions are shown in Fig. 10. The initial \mathbb{M}_{adap} and $\mathbb{M}_{DMP+adap}$ meshes are displayed in Fig. 11. As can be seen, the elements of the $\mathbb{M}_{DMP+adap}$ mesh are aligned along the principle diffusion directions at different places.

Fig. 12 and Fig. 13 show the \mathbb{M}_{adap} mesh and the corresponding numerical solutions at different times, respectively. It is observed that the two free boundaries start merging at around $t = 60$.

Remark 5.3. Due to the challenges of the anisotropic and nonlinear diffusion in the APME, some negative values may occur in the numerical solutions during the computations, which violates the discrete maximum principle (DMP). The cut-off method [25] is applied to force all numerical solutions to be nonnegative. Satisfaction of DMP for APME and the effect of cut-off are under investigation.

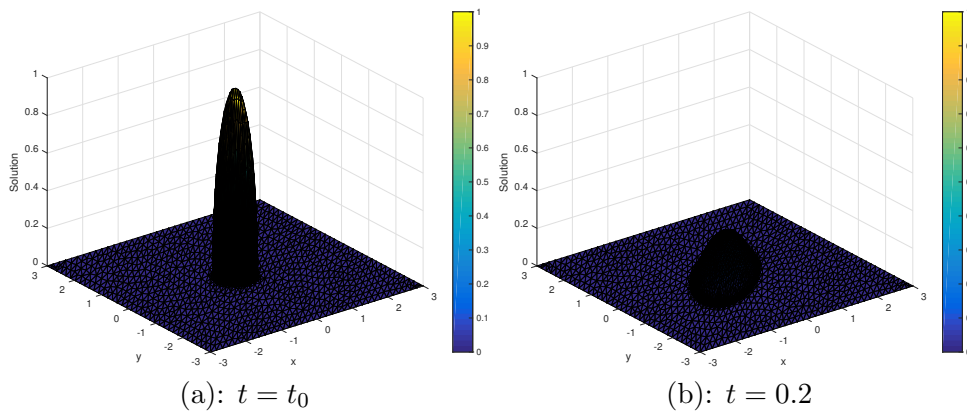


Figure 8: Example 5.2. Initial and final solutions, $m = 1$.

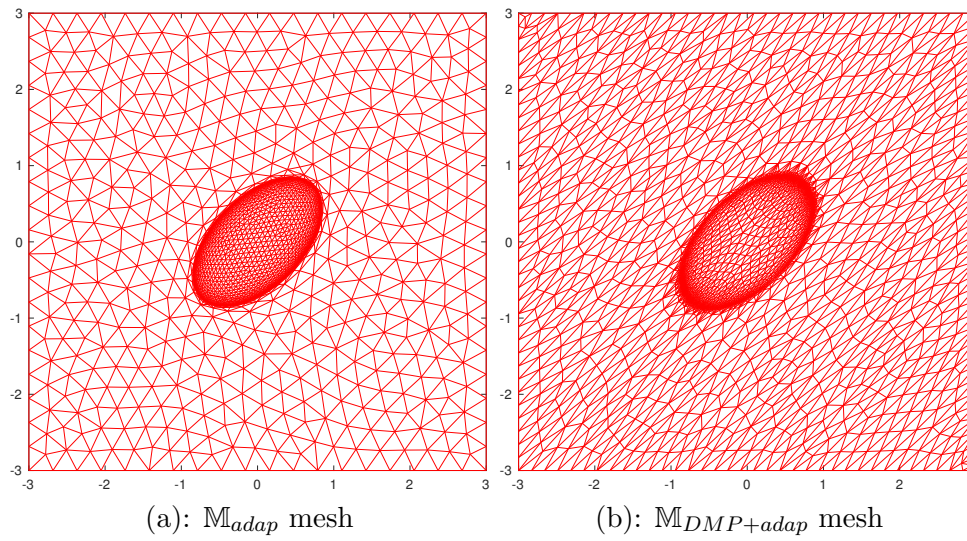


Figure 9: Example 5.2. M_{adap} and $M_{DMP+adap}$ meshes at $t = 0.2$, $m = 2$.

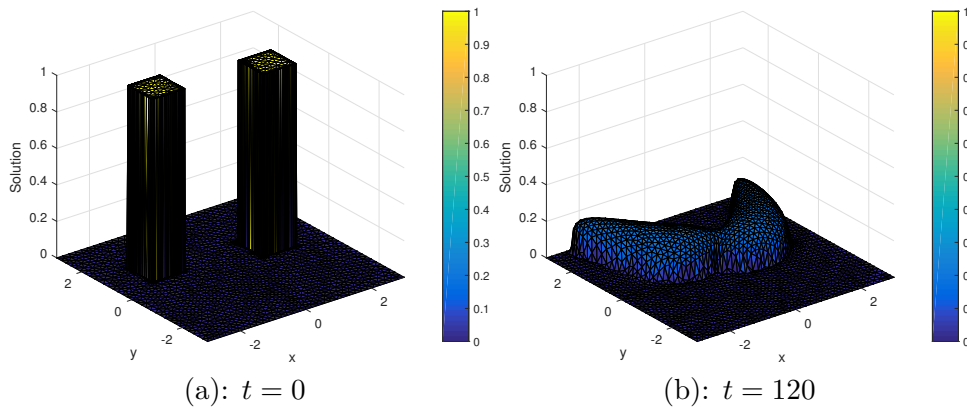


Figure 10: Example 5.3. Initial and final solutions, $m = 6$.

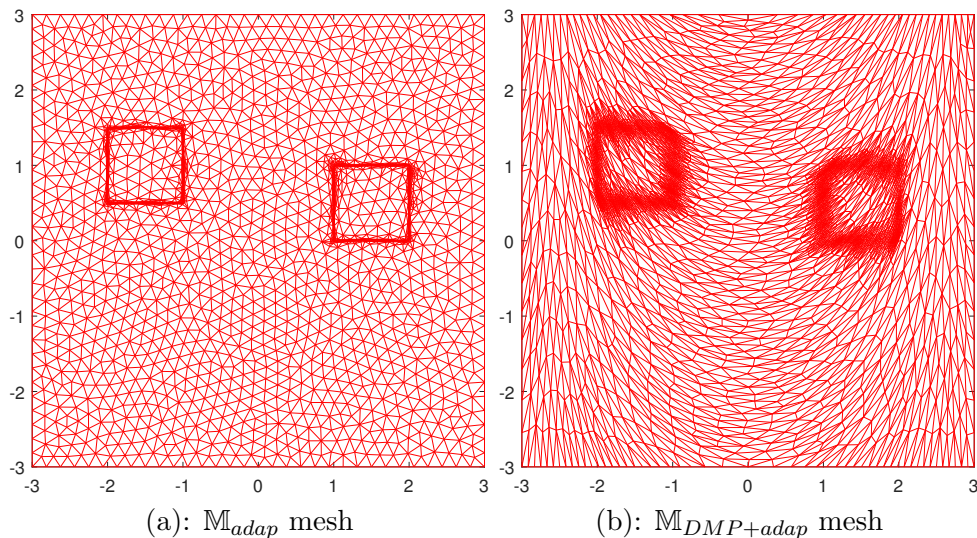


Figure 11: Example 5.3. Initial \mathbb{M}_{adap} and $\mathbb{M}_{DMP+adap}$ meshes, $m = 6$.

6 Summary

In the previous sections, we have generalized the Porous Medium Equation (PME) (2) or (3) to Anisotropic Porous Medium Equation (APME) (10) that takes into account the anisotropy and heterogeneity of the physical properties of the porous media such as permeability. A special exact solution for APME is developed in (17) based on the Barenblatt-Pattle solution (13) for PME.

Meanwhile, anisotropic mesh adaptation technique has been applied to obtain the finite element solutions of APME, which have helped improving both accuracy and efficiency of the computation. For general quasi-uniform meshes, the convergence rate for the solution error can be at mostly first order for $m = 1$. However, with adaptive \mathbb{M}_{adap} mesh or $\mathbb{M}_{DMP+adap}$ mesh, we have attained second order convergence rate, as demonstrated by Example 5.1. Furthermore, for a same metric tensor, better adaptation and smaller errors can be achieved by adjusting the regularization parameter α_h in the computation.

Our result is comparable with those obtained using moving mesh methods in [26] for PME but can achieve the same accuracy with less number of mesh elements. Different than the moving mesh method that keeps the connectivity of the mesh elements, the adaptive meshes, including \mathbb{M}_{adap} and $\mathbb{M}_{DMP+adap}$, not only change the connectivity but also can change the number of elements. Therefore, we can start with a coarse initial uniform mesh and adapt it to concentrate more elements around the free boundaries. The adapted mesh is used as a better initial mesh for later computations.

Numerical results also show different behavior between APME and PME, as demonstrated by Examples 5.1 and 5.2. For PME, the diffusion is the same in all directions, however, for APME, the diffusion is more significant along the principle diffusion direction. The merger between isolated free boundaries also occurs along the principle diffusion directions as demonstrated by Example 5.3. The challenges for general anisotropic diffusion problems also apply to APME such as satisfaction of maximum principle [21, 23, 24]. More investigation on properties of APME is needed.

Acknowledgment. This work was partially supported by the UMRB grant KDM56 (Li) from the University of Missouri Research Board.

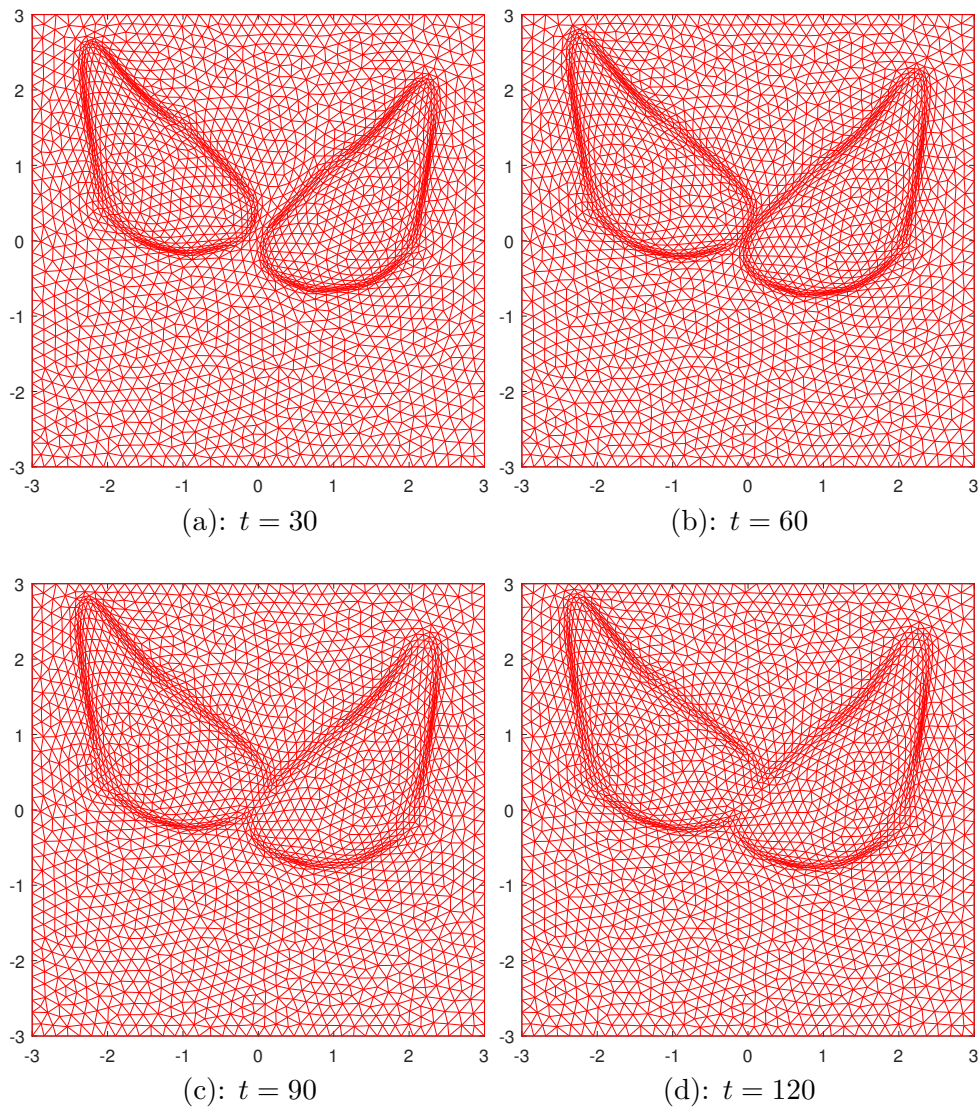


Figure 12: Example 5.3. \mathbb{M}_{adap} meshes at different times, $m = 6$.

References

- [1] D.G. Aronson. Regularity properties of flows through porous media. *SIAM J. Appl. Math.*, 17:461–467, 1969.
- [2] D.G. Aronson, L.A. Caffarelli, and S. S. Kamin. How an initially stationary interface begins to move in porous medium flow. *SIAM J. Appl. Math.*, 14:639–658, 1983.
- [3] G.I. Barenblatt. On some unsteady motions of a liquid or a gas in a porous medium. *Prikl. Mat. Mekh.*, 16 (1):67–78, 1952.
- [4] J. Brandts, S. Korotov, and M. Křížek. The discrete maximum principle for linear simplicial finite element approximations of a reaction-diffusion problem. *Linear Algebra and its Applications*, 429:2344–2357, 2008.

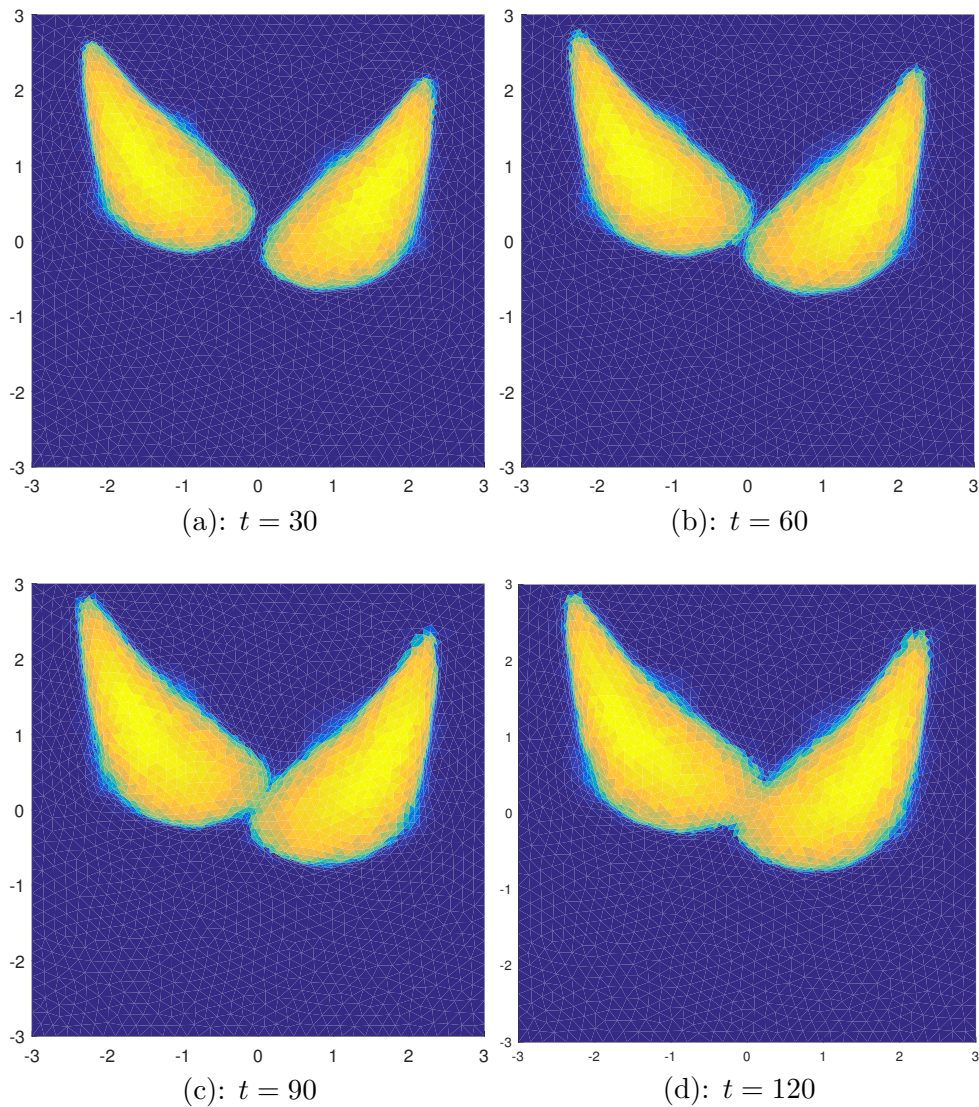


Figure 13: Example 5.3. Numerical solutions using \mathbb{M}_{adapt} meshes at different times, $m = 6$.

- [5] C. Budd, G. Collins, W. Huang, and R.D. Russell. Self-similar numerical solutions of the porous medium equation using moving mesh methods. *Phil. Trans. R. Soc. Lond. A*, 357:1047–1078, 1999.
- [6] E. DiBenedetto and D. Hoff. An interface tracking algorithm for the porous medium equation. *Trans. Amer. Math. Soc.*, 284 (2):463–500, 1984.
- [7] J.C.M. Duque, R.M.P. Almeida, and S.N. Antontsev. Convergence of the finite element method for the porous media equation with variable exponent. *SIAM J. Numer. Anal.*, 51 (6):3483–3504, 2013.
- [8] J.C.M. Duque, R.M.P. Almeida, and S.N. Antontsev. Application of the moving mesh method to the porous medium equation with variable exponent. *Math. Comput. Simulation*, 118:177–185, 2015.

- [9] C. Ebmeyer. Error estimates for a class of degenerate parabolic equations. *SIAM J. Numer. Anal.*, 35(3):1095–1112, 1998.
- [10] C. Ebmeyer and W.B. Liu. Finite element approximation of the fast diffusion and the porous medium equations. *SIAM J. Numer. Anal.*, 46(5):2393–2410, 2008.
- [11] E. Emmrich and D. Siska. Full discretization of the porous medium/fast diffusion equation based on its very weak formulation. *Commun. Math. Sci.*, 10:1055–1080, 2012.
- [12] B.H. Gilting and L.A. Peletier. On a class of similarity solutions of the porous media equation. *J. Math. Anal. Appl.*, 55:351–364, 1976.
- [13] B.H. Gilting and L.A. Peletier. On a class of similarity solutions of the porous media equation ii. *J. Math. Anal. Appl.*, 57:522–538, 1977.
- [14] S. González-Pinto, J.I. Montijano, and S. Pérez-Rodríguez. Two-step error estimators for implicit Runge-Kutta methods applied to stiff systems. *ACM Trans. Math. Softw.*, 30 (1):1–18, 2004.
- [15] F. Hecht. Bidimensional anisotropic mesh generator software (bamg). <https://www.ljll.math.upmc.fr/~hecht/ftp/bamg/bamg-v1.01.tar.gz>, 2010.
- [16] W. Huang. Metric tensors for anisotropic mesh generation. *J. Comput. Phys.*, 204:633–665, 2005.
- [17] W. Huang. Mathematical principles of anisotropic mesh adaptation. *Comm. Comput. Phys.*, 1:276–310, 2006.
- [18] W. Huang and R.D. Russell. *Adaptive Moving Mesh Methods*. Springer, New York, 2011.
- [19] A.S. Kalashnikov. The propagation of disturbances in problems of nonlinear heat conduction with absorption. *USSR Comp. Math. and Math. Phys.*, 14:70–85, 1974.
- [20] L. Kamenski, W. Huang, and H. Xu. Conditioning of finite element equations with arbitrary anisotropic meshes. *Math. Comput.*, 83:2187–2211, 2014.
- [21] D. Kuzmin, M.J. Shashkov, and D. Svyatskiy. A constrained finite element method satisfying the discrete maximum principle for anisotropic diffusion problems. *J. Comput. Phys.*, 228:3448–3463, 2009.
- [22] T.E. Lee, M.J. Baines, and S. Langdon. A finite difference moving mesh method based on conservation for moving boundary problems. *Journal of Computational and Applied Mathematics*, 288:1–17, 2015.
- [23] X. Li and W. Huang. An anisotropic mesh adaptation method for the finite element solution of heterogeneous anisotropic diffusion problems. *J. Comput. Phys.*, 229:8072–8094, 2010.
- [24] X. Li and W. Huang. Maximum principle for the finite element solution of time-dependent anisotropic diffusion problems. *Numer. Meth. PDEs*, 29:1963–1985, 2013.
- [25] C. Lu, W. Huang, and E. VanVleck. The cutoff method for the numerical computation of nonnegative solutions of parabolic PDEs with application to anisotropic diffusion and lubrication-type equations. *J. Comput. Phys.*, 242:24–36, 2013.

- [26] C. Ngo and W. Huang. A study on moving mesh finite element solution of the porous medium equation. *J. Comput. Phys.*, 331:357–380, 2017.
- [27] R.H. Nochetto and C. Verdi. Approximation of degenerate parabolic problems using numerical integration. *SIAM J. Numer. Anal.*, 25(2):784–814, 1988.
- [28] O.A. Oleinik, A.S. Kalashnikov, and Y.-I. Chzou. The cauchy problem and boundary problems for equations of the type of unsteady filtration. *Izv. Akad. Nauk SSR Ser. Math.*, 22:667–704, 1958.
- [29] R.E. Pattle. Diffusion from an instantaneous point source with concentration dependent coefficient. *Quart. Jour. Mech. Appl. Math.*, 12:407–409, 1959.
- [30] I.S. Pop, M. Sepúlveda, F.A. Radu, and O.P. Vera Villagrán. Error estimates for the finite volume discretization for the porous medium equation. *Journal of Computational and Applied Mathematics*, 234:2135–2142, 2010.
- [31] M.E. Rose. Numerical methods for flows through porous media. i. *Mathematics of Computation*, 40 (162):435–467, 1983.
- [32] J. Rulla and N.J. Walkington. Optimal rates of convergence for degenerate parabolic problems in two dimensions. *SIAM J. Numer. Anal.*, 33(1):56–67, 1996.
- [33] G. Scherer and M.J. Baines. Moving mesh finite difference schemes for the porous medium equation. *Mathematics Report Series 1/2012*, pages Department of Mathematics and Statistics, University of Reading, UK, 2012.
- [34] S.I. Shmarev. Interfaces in multidimensional diffusion equations with absorption terms. *Nonlinear Anal.*, 53:791–828, 2003.
- [35] V. Thomée and L.B. Wahlbin. On the existence of maximum principles in parabolic finite element equations. *Math. Comput.*, 77:11–19, 2008.
- [36] J.L. Vázquez. *The porous medium equation - Mathematical theory*. Oxford Mathematical Monographs, The Clarendon Press Oxford University Press, Oxford, 2007.
- [37] D. Wei and L. Lefton. A priori l^p error estimates for Galerkin approximations to porous medium and fast diffusion equations. *Mathematics of Computation*, 68:971–989, 1999.
- [38] Q. Zhang and Z.-L. Wu. Numerical simulation for porous medium equation by local discontinuous Galerkin finite element method. *J. Sci. Comput*, 38:127–148, 2009.